

## ADAPTIVE QUANTIZATION VIA FUZZY CLASSIFIED PRIORITY MAPPING FOR LIVER ULTRASOUND COMPRESSION

RATTIKORN SOMBUTKAEW<sup>1</sup>, ORACHAT CHITSOBHUK<sup>1</sup>  
DUANGKAMON PRAPRUTTAM<sup>2</sup> AND THUMANOON RUANGCHAIJATUPORN<sup>2</sup>

<sup>1</sup>Faculty of Engineering  
King Mongkut's Institute of Technology Ladkrabang  
Chalongkrung Rd., Ladkrabang, Bangkok 10520, Thailand  
ksrattik@hotmail.com; orachatc@yahoo.com

<sup>2</sup>Department of Diagnostic and Therapeutic Radiology  
Faculty of Medicine, Ramathibodi Hospital  
Mahidol University  
Bangkok 10400, Thailand  
radpt@mahidol.ac.th; md\_thum@yahoo.com

Received October 2015; revised January 2016

**ABSTRACT.** *This paper proposes adaptive quantization based on fuzzy classified priority mapping in order to achieve higher encoding efficiency. The priority map serves as a quantization mask, which is adaptively adjusted according to the statistical characteristics in terms of histograms based on the results of Fuzzy C-mean clustering. With its soft clustering property, the results illustrate robustness to ambiguity of the data and thus retain much more information than hard clustering. The priority map represents levels of significance as the Most Significant Group (MSG), the Normal Significant Group (NSG), and the Lowest Significant Group (LSG). The significant candidates of irregular liver tissues requiring special doctor attention will be assigned with higher priority than those from the regular ones. The higher the priority, the greater the number of bits assigned for encoding. An analysis of suitable quantization step size has been conducted. With the selection of appropriate quantization parameters for each priority level, the blocking artifacts can be greatly reduced. This helps to reduce the encoding bit rate and enhance the compression efficiency for the transmission and storage while maintaining an acceptable diagnostic image quality.*

**Keywords:** Ultrasound image compression, Fuzzy C-mean clustering, Adaptive quantization, Priority mapping

**1. Introduction.** With the advance in medical imaging, visual representation of human interior has become massively produced in digital format since the hospitals are moving towards filmless [1] and computer-aid diagnostic processing. The medical information is exchanged from one site to another via electronic communication based on implementation of teleradiology and digital Picture Archiving and Communications Systems (PACS) in order to provide health services with high quality and thus improve patients' health status [2]. The Digital Imaging and Communications in Medicine (DICOM) Standard specifies a non-proprietary data interchange protocol, digital image format, and file structure of biomedical images and image-related information [3]. Liver cancer was reported as the most significant disease causing premature death by the World Health Organization (WHO), especially for the HepatoCellular Carcinoma (HCC). It was also reported as the number one disease found in males and the fifth rank in females by the Ministry of Public Health of Thailand in 2008 [2]. The blood and Alfa-fetoprotein (AFP) tests are recommended as general acceptance test taking for patient diagnosing together with

Ultrasonography (US) in every six months. This introduces a requirement for the massive amount of ultrasound liver images needed to be stored in each hospital's database. In order to handle such massive information, there have been significant considerations in memory requirement and bandwidth limitation for effective DICOM storage and communication. An efficient image compression technique is required to reduce the transmission time and storage cost while preserving the quality of the image. One definition of optimal medical image compression is a degree of compression that decreases file size substantially while producing a degree of image distortion that is not clinically significant [4].

Image compression provides a way to efficiently encode images based on redundancy reduction in order to preserve the actual information resided in the image itself. Transform coding has been popular and widely adopted to transform pixel-wise image representation into a new representation such that the transformed results are independently quantized [5]. Block-based DCT transform is a part of the JPEG standard format. The DCT has been known for near-optimum especially with natural image compression [6]. Each block of subimage is transformed into DC (Direct Current) and AC (Alternating Current) coefficients. DC coefficient expresses the mean value of the subblock while AC coefficients represent zero means with amplitude changes in different frequencies. Most of the energy is compacted in the DC coefficient while details are carried in the AC coefficients. These DCT coefficients are encoded in the form of either lossless or lossy compression techniques. Even though lossless compression allows perfect reconstruction of the original image, it can support Compression Ratio (CR) only up to 4:1 (max) [7]. To achieve higher compression ratio, lossy compression algorithm becomes an alternative selection. The significant constraints for lossy compression are high compression ratio with clinical quality. Context based modeling has been proposed to encode medical image information according to predetermined characteristics [7,9]. ROI based compression is an example of context based compression, where each region is compressed independently with its appropriate compression ratio. The desired compression ratio of each region depends on its significance. The most significant regions are compressed with low compression ratios while the least significant regions are encoded with higher ratios.

The main contribution of this paper is to present adaptive quantization based on Fuzzy C-mean (FCM) clustering for ultrasound liver compression, where the ROIs are classified into three levels of significance: the Most Significant Group (MSG), the Normal Significant Group (NSG), and the Lowest Significant Group (LSG). It serves as a quantization mask, which is adaptively adjusted according to the statistical characteristics in terms of histograms based on the results of FCM. However, the relation between priority level and the suitable quantization scale has not been clearly evaluated. Therefore, another contribution is to provide an analysis of suitable quantization step size related to each priority level. With the appropriate selection of the quantization parameters, the blocking artifacts can be greatly reduced. This helps to reduce the encoding bit rate and enhance the compression efficiency for the transmission and storage while maintaining an acceptable diagnostic image quality.

**2. A Review of Related Works.** Selecting ROI is a challenging task since it affects the overall compression performance for both quality and quantity. Simple maxshift and general scaling were chosen to create ROI based on wavelet based coding in EBCOT of JPEG2000 [8]. The wavelet coefficients of the ROI bit-planes were scaled up so that they were placed in the higher bit-planes in order to give them higher significance [9]. Even though maxshifting allows compression to arbitrarily define ROI shape without ROI mask, the results are not guaranteed lossless compression with a specified bitrate. ROI image

coding using Shape-adaptive DCT was introduced in [9], as a low complexity Shape Adaptive DCT (SA DCT) algorithm suitable for coding arbitrarily shaped image segments. The algorithm encoded the foreground and background of  $8 \times 8$  DCT blocks separately [10-12]. The SA-DCT has been developed in the framework of the ongoing MPEG-4 standardization phase of ISO/IEC and included in the video verification model of MPEG-4. With high computational overhead, an improved version of the SA-DCT called  $\Delta$ DC-SA-DCT was proposed for intraframe coding. It was proven to require smaller computational overhead, thus attractive for hardware implementations [13]. The  $\Delta$ DC-SA-DCT was also adopted as ROI based image coding in [14]. The compression results were compared to the algorithm based on DCT-JPEG. The SA-DCT based coding showed improved compression performance in terms of PSNR and visual quality. However, the limitation of the SA-DCT based coding is that the spatial correlation may be lost due to flushing samples in arbitrarily shaped block to a certain edge of a rectangular bounding block before DCT transformation of row or column, where the coefficients are from different frequency bands [15].

An alternative ROI identification is performed based on segmentation and classification techniques using Vector Quantization (VQ) [16-19], K-mean clustering [20-22], Fractal segmentation [25-27], Support Vector Machine (SVM) [29,30] and Fuzzy C-mean clustering [31,32]. With its lowest quantization distortion at a given bit rate, VQ has been widely adopted for lossy image compression [9,16-19]. Contextual Vector Quantization (CVQ) was proposed to encode an image with different quality between the Contextual Region of Interest (CROI) portion and the Background (BG) for ultrasound images [9]. Region growing was adopted as a segmentation method to define the CROIs. The CROIs were encoded with a low CVQ compression ratio while the BG was encoded with the high CVQ compression ratio. However, in high bit-rate compression, VQ codebooks are relatively large and require extensive computational complexity and memory requirements. K-mean clustering is a clustering technique used to partition data samples into K clusters, where each cluster is indicated by its own center [2,20-22]. In [20], K-mean clustering was adopted for nuclear medical image compression. Clustering without analyzing compression, distortion may result in significant loss of data. Therefore, the segmented image was compared to the original one in all iterations in order to determine the termination criteria. The iteration will be ended when the loss of data is minimized (the value of correlation co-efficient function should be maximum). Statistical calculation and K-mean clustering of motion B-Mode liver ultrasound image were proposed to define approximation of liver position in [23] while differentiating normal regions of the cirrhotic liver was proposed using Law's mask analysis of spatial gray-level dependence matrices, Fourier power spectrum, and gray-level difference [24]. Although implementation of the K-means algorithm is quite simple, the convergence depends on the choice of the initial cluster vector. Fractal based segmentation performs region partitioning using Fractal Dimension (FD) analysis. The FD is a statistical quantity identifying the detail in a pattern, which changes with the scale. Quad-tree partitioning of fractal features was adopted for x-ray images [25]. In [26,27], the ROIs of the mammograms were extracted using fractal based segmentation and then encoded with maxshift ROI coding technique while multiresolution analysis of fractal feature vector for ultrasound liver segmentation was described in [28]. However, the fractal based image coding requires tremendous time for encoding; thus providing poor retrieved image quality when compression is applied on noisy or corrupted images. Another segmentation approach was based on curvelet transform and Support Vector Machine (SVM) regression [29]. The curvelet coefficients were quantized and approximated by SVM with the predefined error. The model parameters of SVM were then encoded with adaptive arithmetic coding. Extensive memory requirement and high computational

complexity are the main drawbacks of SVM for practical implementation [30]. The FCM clustering provides a soft (fuzzy) assignment of patterns (memberships) to clusters [31]. Since each data element can belong to one or more clusters, the levels of memberships can be used to determine the degrees of relationship between data elements and their related clusters. In [32], FCM was introduced as the ROI texture partitioning, where different compression ratios were then assigned the ROIs according to their textural significance. The absolute values of wavelet coefficients for each DWT subband were chosen as texture descriptors.

The ROI classification of liver ultrasound is quite difficult due to the image itself containing other organs, in which their characteristics are closely related to the liver. The hard decision based clustering is not an appropriate choice to cope with this uncertainty. FCM based clustering is suggested in this paper due to its soft decision property. It tries to iteratively optimize the membership function in order to minimize the objective function based on the similarity between the sample data and the cluster center. Each data sample can belong to more than one cluster according to the certain degree of membership [33]. The statistics of different types of liver tissues are illustrated. It can be seen that the texture characteristics of the normal and abnormal tissues are closely related especially in the case of early stage of the disease. With the proposed FCM-based priority clustering, it demonstrates an improvement of the classification for ROIs with ambiguous characteristics of different organs that reside in the image and unstable texture description of liver tissue due to intensity variation of the input image.

**3. Methodology.** JPEG is well known image compression standard based on Discrete Cosine Transform (DCT) [34,35]. There was a study on performance of image compression based on DCT and wavelet for CT scan image [36]. It was concluded that, for a lower compression ratio, DCT based image compression yielded higher quality image than Wavelet. However, the image quality is decreased at higher compression ratios due to the artifacts resulting from the block-based DCT scheme. Figure 1 shows the JPEG encoding process with the proposed adaptive quantization step size.

In JPEG encoding process, an input image is partitioned into consecutive  $8 \times 8$  blocks and each block is transformed using forward DCT algorithm to obtain a set of 64 values of one DC plus 63 AC DCT coefficients. To reduce amount of information, human perception

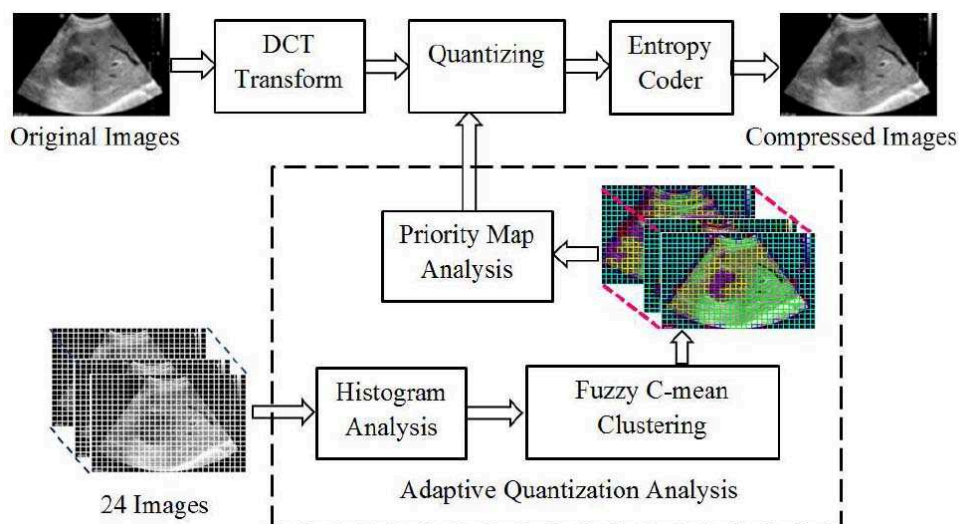


FIGURE 1. The proposed adaptive quantization for JPEG encoding

is taken into consideration. The human visual perception is a complex coordination among the eye, optical nerve, visual cortex and other parts of the brain [37]. The human eye does not perceive directly translation of the retina stimuli, but it involves complicated psychological inference [38]. The psychovisual redundancy is the image information that is ignored by the human visual system or relatively less important to human eye. In another word, the human eye is not equally sensitive to all visual image information [39]. The human visual perception cannot differentiate the difference in brightness over a relatively large area and also in a high frequency of brightness variation. Removing the psychovisual redundancy would be beneficial for image compression. The redundancy elimination is performed through the quantization process via the quantization tables [39]. In JPEG, quantization table is not fixed; however, a standard quantization table  $Q(u, v)_{Classic}$  is recommended as illustrated in Figure 2. This suggested JPEG quantization table is derived based on psychovisual threshold experiments and represents quality of 50%.

-----							
16	11	10	16	24	40	51	61
12	12	14	19	26	58	60	55
14	13	16	24	40	57	69	56
14	17	22	29	51	87	80	62
18	22	37	56	68	109	103	77
24	35	55	64	81	104	113	92
49	64	78	87	103	121	120	101
72	92	95	98	112	100	103	99
-----							

FIGURE 2. The quantization table of standard JPEG

JPEG quantization tables aim to discard the information not visually significant especially at the higher frequencies. A standard quantization equation is presented in (1),

$$F_q(u, v) = \text{Round} \left( \frac{F(u, v)}{Q(u, v)_{Classic}/Q_S(u, v)} \right) \quad (1)$$

where  $F(u, v)$  is the DCT coefficient at  $(u, v)$  spatial frequency in horizontal and vertical directions, respectively,  $Q(u, v)_{Classic}$  is the standard JPEG quantization table (Figure 2) while  $Q_S(u, v)$  is the quantization step size.

JPEG quantization largely determines the rate distortion in a JPEG image compression [40]. Increasing in the quantization leads to increasing the degree of compression; however, the quality of the image would be decreased. The question is the optimization between quality and quantity in terms of compression ratio. Several quantization matrices have been introduced such as for images of human face recognition [41], iris in the human eye [42], and x-ray [43]. However, researchers are still active for alternative optimal quantization.

**3.1. Adaptive quantization.** There was a study of the impact of quantization matrix on the performance of JPEG [44]. From the results, it can be concluded that compression ratio changes when the quantization matrix changes. However, the quality of compression varies from image to image even though the quantization matrix as well as the compression ratio remains the same. This means that each type of images requires a particular quantization, which can be adjusted according to its own characteristic for better compression performance.

In this research, an analysis of adaptive quantization parameters based on FCM classified priority map is presented. Each ultrasound liver image is partitioned into  $32 \times 32$  subimages. The statistical characteristics in terms of histograms are then calculated for each subimage and sent as input training vectors to FCM clustering. A priority map generation is performed according to the clustering results. It identifies the level of importance for each image area and serves as an adaptive quantization mask. The more importance of the image area, the higher value of quantization level.

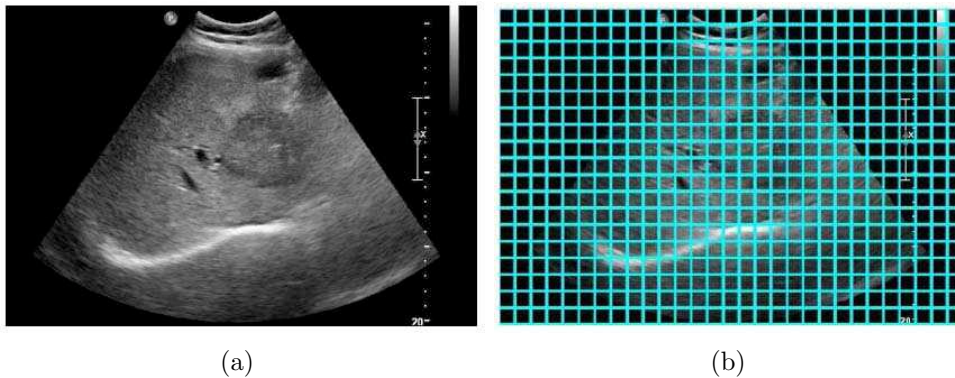


FIGURE 3. (a) Original image ( $928 \times 608$  pixels), (b) subimages with the size of  $32 \times 32$  pixels

3.1.1. *Statistical characteristics of liver tissues.* Histograms are adopted as texture characteristics, which represent the spatial distribution of gray levels and contribute to the perception of texture [45]. Figure 4 illustrates the histograms obtained from various regions in an ultrasound image. Sample regions are abdominal wall in (a), the border of the abnormal liver tissue in (b), the interior of the abnormal liver tissue in (c), Hepatic artery in (d). The gray-level intensity of abdominal wall distributes in a wider range of intensity while the distribution of Hepatic artery is narrower. The abnormal liver tissues both in (b) and (c) illustrate the dominant distribution in a more compact range.

Even though the intensity distribution of abnormal liver tissue demonstrates distinct characteristic, some parts of normal tissues may have the distributions close to the abnormal one especially in the early stage of the disease.

3.1.2. *FCM clustering.* FCM is a soft clustering algorithm, where sub-images can belong to more than one cluster and associated them with a set of membership levels. The Fuzzy C-means (FCM) clustering algorithm was first introduced by Dunn [46] and later extended by Bezdek [47]. The algorithm is an iterative clustering, which creates an optimal partition of  $c$  clusters. Equation (2) is used to minimize the weights within group sum of squared error objective function.

$$J = \sum_{i=1}^c \sum_{j=1}^n (\mu_{ij})^m d^2(X_j, Z_i) \quad (2)$$

where  $J$  is the objective function of FCM algorithm. Let  $x = \{x_1, x_2, \dots, x_n\}$  with  $x_n \in \mathbb{R}^d$  being a data set, which consists of  $N$  dimensional samples, and  $n$  represents the number of data items.  $c$  is the number of clusters.  $m$  is a weighting exponent on each fuzzy membership.  $\mu_{ij}$  is the membership of the  $j^{\text{th}}$  data in the  $i^{\text{th}}$  cluster, and  $Z_i$  is the fuzzy cluster centroid of the  $i^{\text{th}}$  cluster [48].

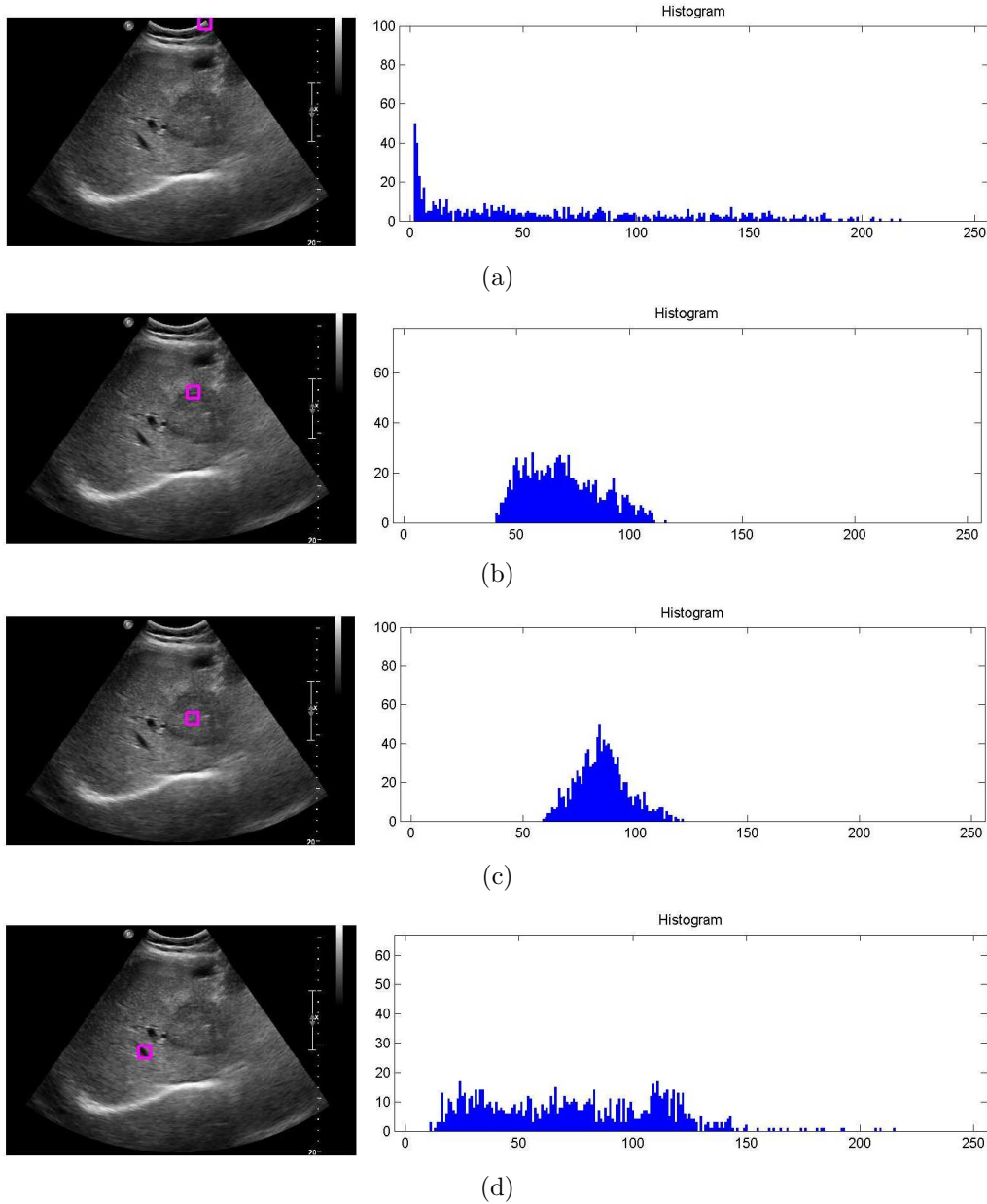


FIGURE 4. Histograms of sample regions in ultrasound liver image, (a) abdominal wall, (b) the border of the abnormal liver tissue, (c) the interior of the abnormal liver tissue, (d) Hepatic artery

Using the Euclidean norm, Equation (3) is the distance metric  $d$  that measures the similarity between a feature vector  $X_j$  and a cluster centroid  $Z_i$  in the feature space.

$$d^2(X_j, Z_i) = \|X_j - Z_i\|^2 \quad (3)$$

The objective function is minimized when data points are close to the centroid of their clusters, which will be assigned with high membership values. On the other hand, low membership values are assigned to data points far from the centroid. Equation (4) is membership function. Equation (5) is updated cluster centroids.

$$u_{ij} = \left( \sum_{k=1}^c \left( \frac{d(x_j, v_i)}{d(x_j, v_k)} \right)^{2/(m-1)} \right)^{-1} \quad (4)$$

$$Z_i = \frac{\sum_{j=1}^n (\mu_{ij})^m X_j}{\sum_{j=1}^n (\mu_{ij})^m} \quad (5)$$

The FCM algorithm proceeds by iterating the two necessary conditions until a solution is reached [49]. Each data point will be associated with a membership value for each class after FCM clustering. The data point will be assigned the class label according to the highest membership value. The important parameters of FCM are the number of clusters ( $c$ ), the weighting exponent ( $m$ ), and termination criteria [50]. When clustering real data without any a priori information about the structures in the data, one usually has to make assumptions about the number of underlying clusters. The fuzziness parameter in terms of the weighting exponent  $m$  significantly influences the fuzziness of the resulting partition. Usually,  $m = 2$  is initially chosen. The FCM algorithm terminates when the norm of the difference between  $\mathbf{U}$  in two successive iterations is smaller than the termination parameter  $\varepsilon = 10^{-6}$ .

**3.1.3. Quantization based on a priority map.** To accommodate the variation in image statistics, the quantization step size is needed to be adaptively adjusted in order to achieve higher encoding efficiency. In this research, the quantization step size is modified according to a priority map created from the clustering results. The priority map generation is a process to create an adaptive quantization mask. It specifies the levels of significance as the Most Significant Group (MSG), the Normal Significant Group (NSG), and the Lowest Significant Group (LSG) according to the results of FCM. The significant sub-images from the candidates of irregular liver tissues, which need special doctor's attention, will be assigned with higher priority than those from the regular ones. The higher the priority, the greater number of bits assigned for encoding. A standard quantization equation is presented in (6).

$$F_q(u, v) = \text{Round} \left( \frac{F(u, v)}{Q(u, v)_{\text{Classic}}/Q_S(u, v)} \right) \quad (6)$$

where  $Q(u, v)_{\text{Classic}}$  is the standard JPEG quantization table (Figure 2) while  $Q_S(u, v)$  is the proposed quantization step size in (7).

$$Q_S(u, v) = \begin{cases} Q_L & LSG \\ Q_N & NSG \\ Q_M & MSG \end{cases} \quad (7)$$

The quantization step of  $Q_M$  is assigned to the Most Significant Group (MSG), which represents the candidate of irregular liver tissues. The normal tissues, the border of the probe, and the scale/color bars are grouped into the Normal Significant Group (NSG), which will be assigned the quantization step of  $Q_N$ . The Lowest Significant Group (LSG) is considered as the lowest priority in the priority map, where sub-images of this class are quantized to the minimum number of encoding bits. Figure 5 presents (a) the ground truth image with the irregular tissue located within the red circle area and (b) the classification results from Fuzzy C-mean clustering. Analysis of optimal quantization step for each priority level should be performed in order to achieve the greatest performance.

**4. Results and Discussions.** In this research, a set of 17 abnormal and 7 normal liver ultrasound images is used for analysis. An ultrasound image is partitioned into sub-images of size  $32 \times 32$  pixels. A 256-bin histogram of each sub-image is then calculated. Since the gray-level distributions of normal and abnormal tissues are overlapped, especially in the case of early stage, it would be difficult to efficiently cluster using hard clustering such

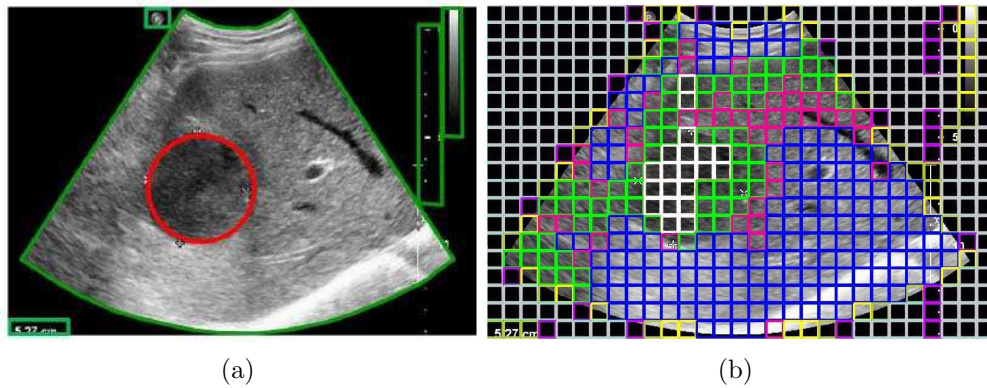


FIGURE 5. (a) The ground truth image with the irregular tissue located within the circle area at the middle and (b) the classified sub-images, where the white sub-images are for the MSG, the light gray sub-images are for the LSG, and the rest sub-images are for the NSG

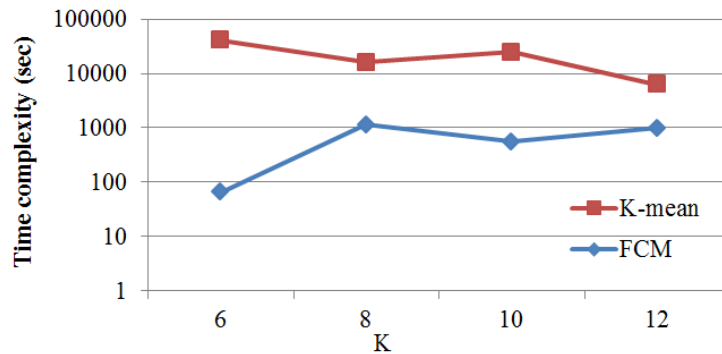


FIGURE 6. A comparison of time complexity of K-mean and FCM clustering (logarithmic scale)

as K-mean. This results in expanding time to achieve clustering results. To overcome this difficulty, Fuzzy C-mean soft clustering is implemented. The cluster centers and membership values are iteratively updated. Using fuzzy membership allows FCM to be robust to noise and outliers and gives superior clustering performance. A comparison of time complexity of K-mean and FCM clustering is conducted as illustrated in Figure 6. The clustering parameters for  $K = 6, 8, 10,$  and  $12$  are evaluated using Matlab functions of K-mean and FCM. The sample results of K-mean and FCM clustering are shown in Figures 7 and 8. From the results, it can be seen that FCM soft clustering produces better clustering results with remarkably faster convergence than the K-mean hard clustering. From experiments, the number of clusters ( $K = 10$ ) can achieve better clustering performance with reasonable time complexity.

The results obtained from FCM clustering are then used to construct a priority map, which specifies the level of importance of the liver tissue regions. The highest priority map designated as the MSG is compressed with higher compression ratio than the lower priority map denoted as the NSG. An analysis of appropriate quantization step sizes ( $3 \leq Q_S \leq 12$ ) for MSG with  $Q_N = 2$  and  $Q_L = 0$  for NSG and LSG respectively is conducted. Figure 9 presents the sample results of reconstructed images using the standard quantization table (c) and using quantization step sizes of 3 (d) and 6 (e) respectively. In order to reduce

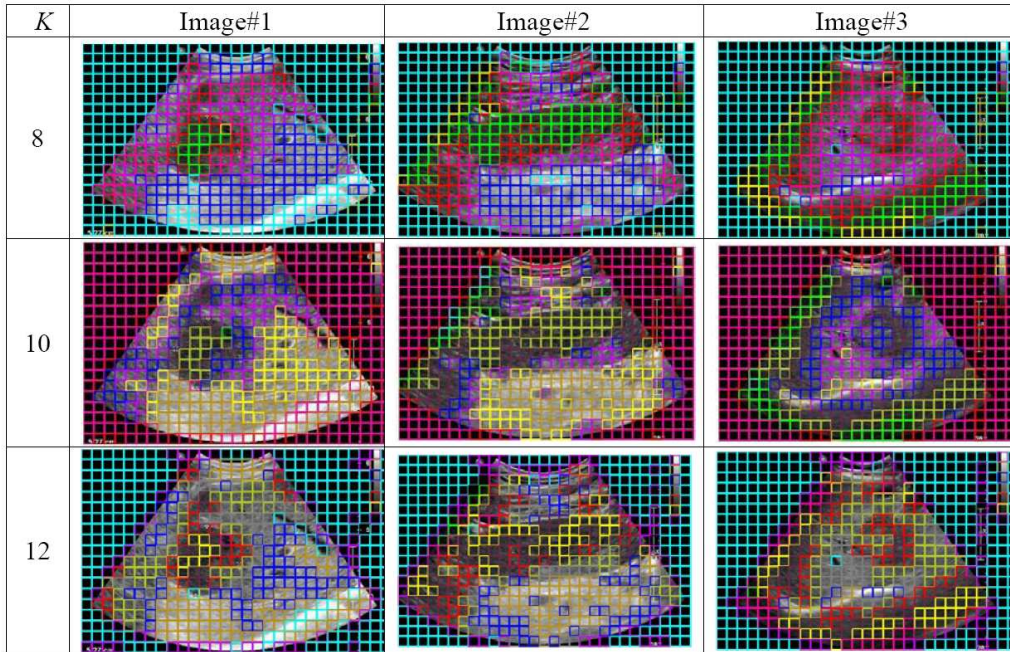


FIGURE 7. The sample results of K-mean clustering for  $K = 8, 10, 12$

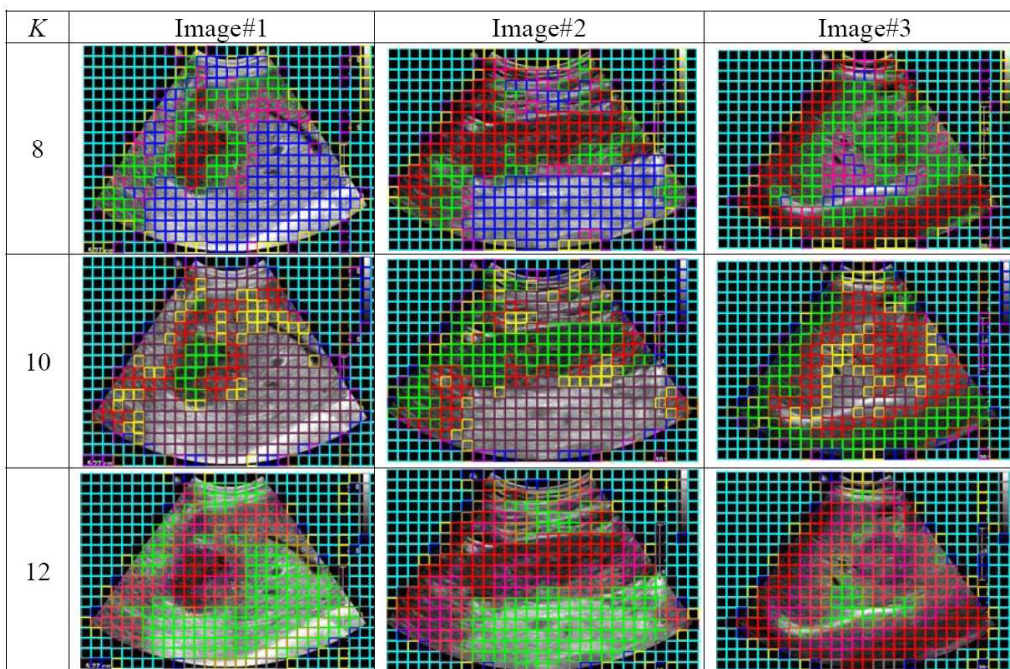


FIGURE 8. The sample results of FCM clustering for  $K = 8, 10, 12$

the blocking artifacts, the quantization step size needs to be increased. The greater value of the quantization step size, the higher quality of the reconstructed image.

The objective measurement in terms of Peak Signal to Noise Ratio (PSNR) [51], Weighted Signal to Noise Ratio (WPSNR) [52], and Structural Similarity (SSIM) [53] are adopted, which can be calculated as presented in (8) and (10) respectively.

$$WPSNR = 10 \log_{10} \frac{MAX_I^2}{MSE \times NVF^2} \quad (8)$$

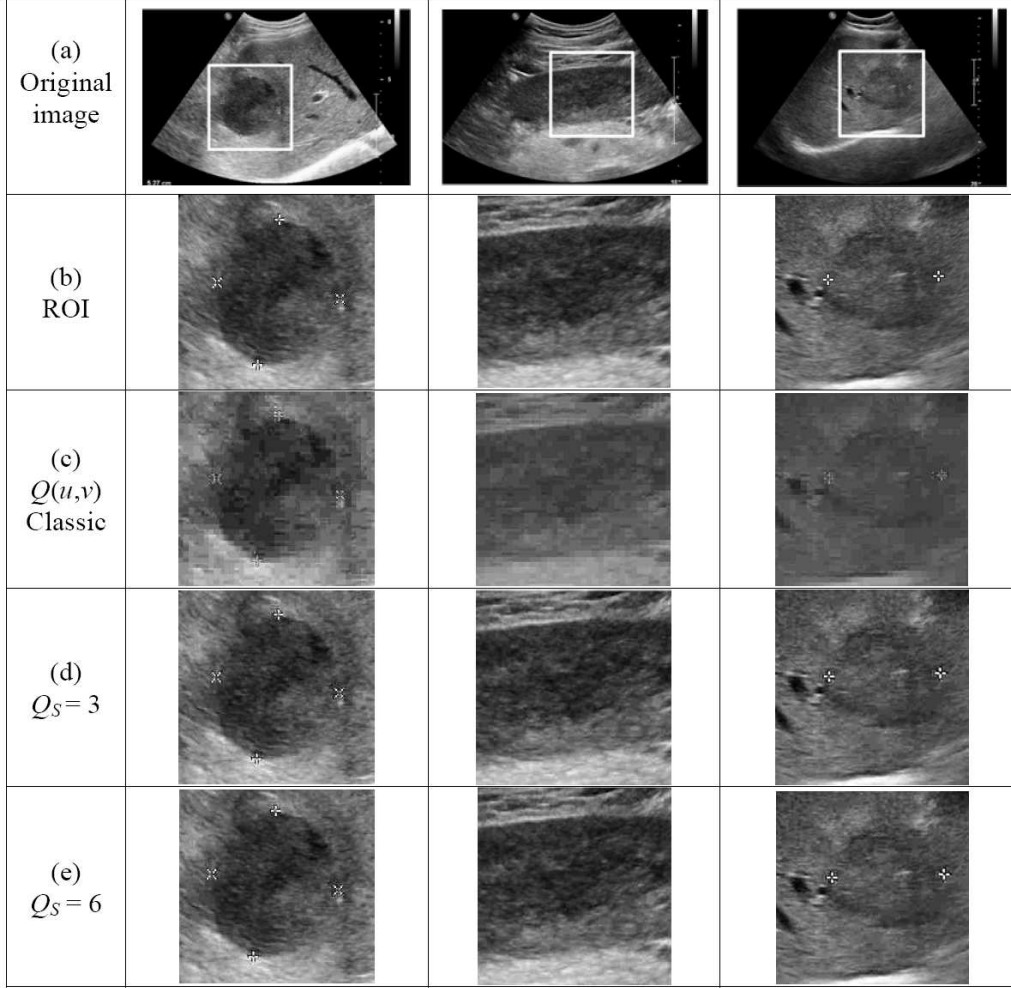


FIGURE 9. The sample results of reconstructed images: (a) the original image containing the abnormal tissue in white region, (b) the region of interest (ROI), (c)-(e) the compressed images with the standard quantization  $Q(u,v)_{Classic}$ , the proposed adaptive quantization with  $Q_S(u,v)_{FCM(K=10)} = 3$  and  $Q_S(u,v)_{FCM(K=10)} = 6$ , respectively

$$NVF(i, j) = \frac{1}{1 + Q_x^2(i, j)} \quad (9)$$

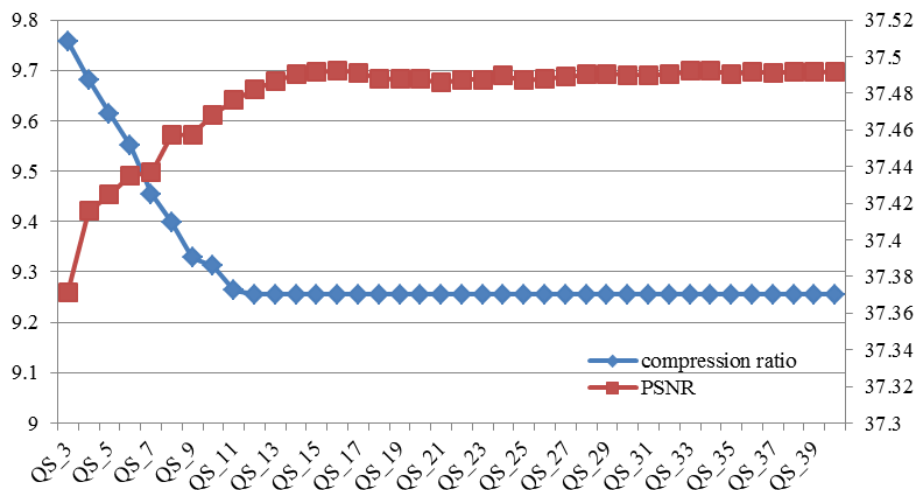
$$SSIM(x, y) = \frac{(2\mu_x\mu_y + C_1)(2\sigma_{xy} + C_2)}{(\mu_x^2 + \mu_y^2 + C_1)(\sigma_x^2 + \sigma_y^2 + C_2)} \quad (10)$$

where  $MAX_I$  is maximum intensity in the image.  $MSE$  is mean square error.  $NVF(i, j)$  is Noise Visibility Function.  $\mu_x$  and  $\mu_y$  are the average of pixel  $x$  and  $y$ .  $Q_x^2(i, j)$  is Local variance.  $\sigma_x^2$  and  $\sigma_y^2$  are the variance of pixel  $x$  and  $y$ .  $C$  is constant.

One of the well-known parameters used to measure image quality is PSNR, which measures the level of similarity between reconstructed image and the original one. WPSNR has been proposed as an alternative image quality measurement to PSNR with additional NVF texture masking function. The Gaussian model is adopted in the NVF to estimate amount of texture in an image. SSIM is another image quality measurement, which calculates luminance, contrast, and structure comparison in terms of the mean and variance of a pixel with its neighbors. Table 1 illustrates objective measurement comparison in terms of PSNR, WPSNR, and SSIM. Large objective measurement leads to better image

TABLE 1. Average objective measurement of liver ultrasound image compression

$Q_S$	PSNR	WPSNR	SSIM	$Q_S$	PSNR	WPSNR	SSIM
3	37.37118	13.86961	0.34495	22	37.48740	13.86981	0.34496
4	37.41576	13.86932	0.34495	23	37.48753	13.86983	0.34496
5	37.42482	13.86982	0.34496	24	37.48955	13.86965	0.34496
6	37.43506	13.86957	0.34495	25	37.48704	13.86984	0.34496
7	37.43681	13.86970	0.34495	26	37.48804	13.86980	0.34496
8	37.45731	13.86922	0.34496	27	37.48917	13.86983	0.34496
9	37.45744	13.86975	0.34496	28	37.49022	13.86979	0.34496
10	37.46826	13.86969	0.34496	29	37.49046	13.86987	0.34496
11	37.47625	13.86976	0.34496	30	37.49003	13.86980	0.34496
12	37.48228	13.86967	0.34496	31	37.49001	13.86980	0.34496
13	37.48639	13.86983	0.34496	32	37.49026	13.86986	0.34496
14	37.49045	13.86976	0.34496	33	37.49209	13.86988	0.34496
15	37.49151	13.86985	0.34496	34	37.49214	13.86985	0.34496
16	37.49264	13.86987	0.34496	35	37.49065	13.86983	0.34496
17	37.49127	13.86984	0.34496	36	37.49145	13.86983	0.34496
18	37.48790	13.86976	0.34496	37	37.49121	13.86981	0.34496
19	37.48763	13.86985	0.34496	38	37.49161	13.86988	0.34496
20	37.48765	13.86977	0.34496	39	37.49141	13.86984	0.34496
21	37.48595	13.86982	0.34496	40	37.49197	13.86984	0.34496

FIGURE 10. An analysis of the appropriate value of  $Q_S$  is conducted in terms of PSNR versus compression ratio.

quality. Even though both WPSNR and SSIM try to model human visual perception, their values cannot be clearly distinguished two images with different qualities compared to the traditional PSNR especially for the images with high texture characteristics such as the ultrasound images.

Compression ratio is another parameter used to measure the ability to reduce the size of the compressed image from the size of the original image. PSNR indicates the loss of information in the image while the compression ratio specifies the degree of compression. Nevertheless, compromising between quality and compression ratio is a critical issue. Although increasing MSG quantization step size ( $Q_S$ ) will enhance quality in terms of

PSNR, the compression ratio will be reduced obviously. An analysis of the appropriate value of  $Q_S$  versus compression ratio is conducted and illustrated in Figure 10.

As a result, the intersection point between PSNR and compression ratio is suggested to be a target point, which lies at  $Q_S = 7$ . However, at  $Q_S = 6$ , the value of the compression ratio is quite larger than at  $Q_S = 7$  while the value of PSNR is not much different. Therefore,  $Q_S = 6$  would be a better choice. With  $Q_S = 6$ , the quality in terms of PSNR is improved by 3.86 dB while the storage saving is reduced by 4.53% compared to the standard quantization. The results show great improvement of the reconstructed images while maintaining acceptable compression ratio.

**5. Conclusions.** This research proposes adaptive quantization for liver ultrasound image compression. The quantization step size is adaptively adjusted according to the fuzzy classified priority map. An ultrasound image is partitioned into sub-images and their statistical characteristics in terms of histograms are extracted as key features for Fuzzy C-mean soft clustering. The clustering results are used to construct the priority mapping, which specified the levels of importance for each image area. The higher the priority, the greater the number of bits assigned for encoding. An analysis of suitable quantization step size has been conducted. With the selection of appropriate quantization parameters, the blocking artifacts can be greatly reduced. Several subjective measurements are evaluated to demonstrate the performance of the proposed algorithm compared to the standard JPEG. The results indicate quality improvement of the reconstructed images while the compression ratio remains reasonably high.

**Acknowledgment.** Ultrasound liver images were supported by the Department of Diagnostic and Therapeutic Radiology, Faculty of Medicine, Ramathibodi Hospital, Mahidol University, Bangkok, Thailand.

## REFERENCES

- [1] S. Sridevi, V. R. Vijayakumar and R. Anuja, A survey on various compression methods for medical images, *I. J. Intelligent Systems and Applications*, vol.3, pp.13-19, 2012.
- [2] R. Sombutkaew, Y. Kumsang and O. Chitsobuk, Adaptive quantization with fuzzy c-mean clustering for liver ultrasound compression, *The 14th International Conference on Control, Automation and Systems (ICCAS 2014)*, Seoul, South Korea, pp.521-524, 2014.
- [3] W. D. Bidgood, S. C. Horii, F. W. Prior and D. E. Van Syckle, Understanding and using DICOM, the data interchange standard for biomedical imaging, *Journal of the American Medical Informatics Association*, vol.4, no.3, pp.199-212, 1997.
- [4] A. C. Flint, Determining optimal medical image compression: Psychometric and image distortion analysis, *BMC Medical Imaging*, pp.1-7, 2012.
- [5] T. Uehara, R. Safavi-Naini and P. Ogunbona, Recovering DC coefficients in block-based DCT, *IEEE Transactions on Image Processing*, vol.15, no.11, pp.3592-3596, 2006.
- [6] N. R. Thota and S. K. Devireddy, Image compression using discrete cosine transform, *Georgian Electronic Scientific Journal: Computer Science and Telecommunications*, no.3, pp.35-43, 2008.
- [7] M. A. Ansari and R. S. Anand, Recent trends in image compression and its application in telemedicine and teleconsultation, *XXXII National Systems Conference*, pp.59-64, 2008.
- [8] C. Christopoulos, J. Askelöf and M. Larsson, Efficient methods for encoding regions of interest in the upcoming JPEG2000 still image coding standard, *IEEE Signal Processing Letters*, vol.7, no.9, pp.247-249, 2000.
- [9] S. M. Hosseini and A.-R. Naghsh-Nilchi, Medical ultrasound image compression using contextual vector quantization, *Computers in Biology and Medicine*, pp.743-750, 2012.
- [10] T. Sikora and B. Makai, Shape-adaptive DCT for generic coding of video, *IEEE Transactions on Circuits and Systems for Video Technology*, vol.5, no.1, pp.59-62, 1995.
- [11] T. Sikora, Low complexity shape-adaptive DCT for coding of arbitrarily shaped image segments, *Signal Processing: Image Communication*, pp.381-395, 1995.

- [12] C. S. Fabregas and N. P. Tri, Ultrasound image coding using shape-adaptive DCT and adaptive quantization, *Infoscience EPFL*, 1997.
- [13] P. Kauff and K. Schuur, Shape-adaptive DCT with block-based DC separation and  $\Delta$ DC correction, *IEEE Transactions on Circuits and Systems for Video Technology*, vol.8, no.3, pp.237-242, 1998.
- [14] Y. Zheng, X. Wang and C. Wang, Shape-adaptive DCT and its application in region-based image, *International Journal of Signal Processing, Image Processing and Pattern Recognition*, vol.7, no.1, pp.99-108, 2014.
- [15] S. Li and W. Li, Shape adaptive discrete wavelet transforms for arbitrarily shaped visual object coding, *Microsoft Research*, pp.1-28, 2000.
- [16] A. I. Gonzalez, M. Grana, J. R. Cabello, A. D'Anjou and F. X. Albizuri, Experimental results of an evolution based strategy for VQ image filtering, *Information Sciences*, pp.249-266, 2001.
- [17] N. Sanyal, A. Chatterjee and S. Munshi, Modified bacterial foraging optimization technique for vector quantization-based image compression, *Computational Intelligence in Image Processing*, pp.131-152, 2013.
- [18] K. Sasazaki, S. Saga, S. Maeda and V. Suzuki, Vector quantization of images with variable block size, *Applied Soft Computing*, vol.8, pp.634-645, 2008.
- [19] W.-J. Hwang, B.-Y. Ye and S.-C. Liao, A novel entropy-constrained competitive learning algorithm for vector quantization, *Neurocomputing*, pp.133-147, 1999.
- [20] H. N. Moulick and M. Ghosh, Image compression using k-means clustering and nuclear medical image processing, *International Journal of Innovative Research in Computer and Communication Engineering*, vol.1, no.4, pp.869-877, 2013.
- [21] R. Harikumar, B. V. Kumar and G. Karthick, Performance analysis for quality measures using k-means clustering and EM models in segmentation of medical images, *International Journal of Soft Computing and Engineering*, vol.1, pp.74-80, 2012.
- [22] A. A. Adebisi, O. E. Olusayo and O. S. Olatunde, An exploratory study of k-means and expectation maximization algorithms, *British Journal of Mathematics & Computer Science*, pp.62-71, 2012.
- [23] C. K. Lin, F. C. Lin, F. L. Lian, K. H. Chang, M. C. Ho, J. Y. Yen and Y. Y. Chen, Ultrasound image-guided algorithms for tracking liver motion, *IEEE/ASME International Conference on Advanced Intelligent Mechatronics*, pp.51-56, 2012.
- [24] C. M. Yu, Y. C. Chen and K. S. Hsieh, Texture features for classification of ultrasonic liver images, *IEEE Transactions on Medical Imaging*, vol.11, no.2, pp.141-152, 1992.
- [25] F. Khalili, M. Celenk and A. Akinlar, Medical image compression using quad-tree fractals and segmentation, *Proc. of the 2013 World Congress in Computer Science, Computer Engineering, and Applied Computing*, 2013.
- [26] B. Grinstead, H. Sari-Sarraf, S. Gleason and S. Mitra, Content-based compression of mammograms for telecommunication and archiving, *Proc. of CBMS*, pp.37-42, 2000.
- [27] B. Grinstead, *Content-based Compression of Mammograms*, Master Thesis, Texas Tech University, 2001.
- [28] W. L. Lee, Y. C. Chen, Y. C. Chen and K. S. Hsieh, Unsupervised segmentation of ultrasonic liver images by multiresolution fractal feature vector, *Information Sciences: An International Journal*, vol.175, pp.177-199, 2005.
- [29] Y. Li, Q. Yang and R. Jiao, Image compression scheme based on curvelet transform and support vector machine, *Expert Systems with Applications*, pp.3063-3069, 2010.
- [30] L. Auria and R. A. Moro, *Support Vector Machines (SVM) as a Technique for Solvency Analysis*, Discussion Paper, DIW Berlin German Institute for Economic Research, pp.1-16, 2008.
- [31] B. Aaron, D. E. Tamir, N. D. Rishe and A. Kandel, Dynamic incremental fuzzy c-means clustering, *The 6th International Conferences on Pervasive Patterns and Applications*, pp.28-37, 2014.
- [32] D. A. Karras, S. A. Karkanis and D. E. Maroulis, Efficient image compression of medical images using the wavelet transform and fuzzy c-means clustering on regions of interest, *IEEE*, pp.469-473, 2000.
- [33] M. Hassan, A. Chaudhry, A. Khan and M. A. Iftikhar, Robust information gain based fuzzy c-means clustering and classification of carotid artery ultrasound images, *Computer Methods and Programs in Biomedicine*, vol.113, no.2, pp.593-609, 2014.
- [34] W. B. Pennebaker and J. L. Mitchell, *JPEG: Still Image Data Compression Standard*, Van Nostrand Reinhold, New York, 1993.
- [35] A. M. Raid, W. M. Khedr, M. A. El-dosuky and W. Ahmed, JPEG image compression using discrete cosine transform – A survey, *International Journal of Computer Science & Engineering Survey (IJCSSES)*, vol.5, no.2, pp.39-47, 2014.

- [36] S. Jabbar and S. Panchikkil, Lossy compression schemes based on transforms – A literature review on medical images, *International Journal of Advanced Information Technology*, vol.2, no.6, pp.25-31, 2012.
- [37] R. J. Strenberg, *Cognitive Psychology*, 3rd Edition, Thomson Wadsworth, 2003.
- [38] G. Zhai, X. Wu, X. Yang, W. Lin and W. Zhang, A psychovisual quality metric in freeenergy principle, *IEEE Transactions on Image Processing*, vol.21, no.1, pp.41-52, 2012.
- [39] F. Ernawan, N. A. Abu and N. Suryama, TMT quantization table generation based on psychovisual threshold for image compression, *International Conference of Information and Communication Technology*, pp.202-207, 2013.
- [40] E. H. Yang and L. Wang, Joint optimization of run-length coding, Huffman coding, and quantization table with complete baseline JPEG decoder compatibility, *IEEE Transactions on Image Processing*, vol.18, no.1, pp.63-74, 2009.
- [41] G.-M. Jeong, C. Kim, H.-S. Ahn and B.-J. Ahn, JPEG quantization table design for face images and its application to face recognition, *IEICE Transaction Fundamentals*, vol.89, no.11, 2006.
- [42] G. S. Kostmajer, H. Stogner and A. Uhl, Custom JPEG quantization for improved iris, *IFIP International Federation for Information Processing*, pp.76-86, 2009.
- [43] A. J. Maeder, Tuning of JPEG quantization matrices for x-ray images, *Proc. of SPIE3031, Medical Imaging 1997: Image Display*, 1997.
- [44] S. V. Viraktamath and G. V. Attimarad, Impact of quantization matrix on the performance of JPEG, *International Journal of Future Generation Communication and Networking*, vol.4, no.3, pp.107-118, 2011.
- [45] G. Malathi and V. Shanthi, Histogram based classification of ultrasound images of placenta, *International Journal of Computer Applications*, vol.1, no.16, pp.49-53, 2010.
- [46] J. C. Dunn, A fuzzy relative of the ISODATA process and its use in detecting compact well-separated clusters, *Journal of Cybernetics and Systems*, vol.3, pp.32-57, 1973.
- [47] J. C. Bezdek, *Pattern Recognition with Fuzzy Objective Function Algorithms*, Plenum Press, New York, 1981.
- [48] S. H. Berenjabad, A. Mahloojifar and A. Akhavan, Threshold based lossy compression of medical ultrasound images using contourlet transform, *The 18th Iranian Conference on BioMedical Engineering*, Tehran, Iran, pp.191-194, 2011.
- [49] J. Wang, J. Kong, Y. Lub, M. Qi and B. Zhang, A modified FCM algorithm for MRI brain image segmentation using both local and non-local spatial constraints, *Computerized Medical Imaging and Graphics*, pp.685-698, 2008.
- [50] U. Kaymak and R. Babuska, *4 Fuzzy Clustering*, [homes.di.unimi.it/.../Fuzzy-Clustering-lecture-Babuska.pdf](http://homes.di.unimi.it/.../Fuzzy-Clustering-lecture-Babuska.pdf), pp.55-72, 1995.
- [51] P. Telagarapu, V. J. Naveen, A. L. Prasanthi and G. V. Santhi, Context based medical image compression with application to ultrasound images, *International Journal of Signal Processing, Image Processing and Pattern Recognition*, vol.4, no.3, pp.61-74, 2011.
- [52] K. A. Navas, D. K. G. Gayathri, M. S. Athulya and A. Vasudev, MWPSNR: A new image fidelity metric, *Recent Advance in Intelligent Computation Systems*, pp.627-632, 2011.
- [53] Z. Wang, A. C. Bovik, H. R. Sheikh and E. P. Simoncelli, Image quality assessment from error visibility to structural similarity, *IEEE Transactions on Image Processing*, vol.13, no.4, pp.600-612, 2004.